Surface roughness of stainless-steel mirrors for focusing soft x rays

Valeriy V. Yashchuk, Eric M. Gullikson, Malcolm R. Howells, Steve C. Irick, Alastair A. MacDowell, Wayne R. McKinney, Farhad Salmassi, Tony Warwick, James P. Metz, and Thomas W. Tonnessen

We have used polished stainless steel as a mirror substrate to provide focusing of soft x rays in grazing-incidence reflection. The critical issue of the quality of the steel surface, polished and coated with gold, is discussed in detail. A comparison is made to a polished, gold-coated, electroless nickel surface, which provides a smoother finish. We used the surface height distributions, measured with an interferometric microscope and complemented by atomic-force microscope measurements, to compute power spectral densities and then to evaluate the surface roughness. The effects of roughness in reducing the specular reflectivity were verified by soft-x-ray measurements. © 2006 Optical Society of America

OCIS codes: 120.6660, 220.4880, 220.5450, 240.5770, 340.7470.

1. Introduction

Shaped mirrors are commonly used in pairs[1–20] at synchrotron radiation facilities for focusing x rays in experiments. These mirrors typically reflect horizontally and vertically, each focusing in one plane. They are often used at high demagnification to generate a small x-ray spot and tangentially should have an elliptical surface. Bending mechanisms for this type of mirror have been extensively studied.[21–27] They must provide a tuned bending couple at each end of the mirror substrate, which would give a linear variation of curvature from one end of a uniform substrate to the other. One generates the required correction to achieve an elliptically bent shape by varying the width (or thickness) of the substrate as a function of its length. The effects of gravity can be made negligible by a second iteration of this variation.[15] The resultant optical systems have been reported to deliver illumination spots limited by the polished quality of the substrate.[15] If they are used at short working distances, the x-ray spots can be smaller than 1 μm.[28] To keep the mirrors short, one should use them with grazing angles as large as the x-ray reflectivity will allow. For soft x rays with energies below 2 keV, the grazing angle may be larger than 1.5°. An undulator beam can easily be collected at the end of a typical 30 m soft-x-ray beam line by a mirror that is 300 mm long. The required bending radii may be as small as 20 m, and the stresses will then exceed the capabilities of conventional glass and silicon substrates. Metal is preferred, both for its strength and for its ease of attachment, in systems that must be baked for ultrahigh vacuum and must necessarily be ultraclean. We used copper in the past[15] with an electroless nickel surface for smooth polishing. Stainless steel is stronger and can be polished directly. However, it is not clear how smooth the finished steel surface can be. These mirrors require an optical coating, usually of gold or platinum, but at the proper thickness this coating conforms to the finish and figure of the underlying polished surface.

In this paper we report on a finish achieved on a suite of three stainless-steel (SS) mirrors recently installed at beam line 11.0.1 at the Advanced Light Source (ALS), Lawrence Berkeley National Laboratory. The mirror's surface roughness was greater than desired, but the mirrors were smooth enough for successful installation and use. One of these three SS mirrors was plated with electroless nickel after the steel failed to polish sufficiently smooth. This extra production step provided a surface that could be polished smooth while it retained the strength of the underlying steel. We show measurements of roughness, scattering, and reflectivity, both from gold-

V. V. Yashchuk (vvyashchuk@lblgov), E. M. Gullikson, M. R. Howells, S. C. Irick, A. A. MacDowell, W. R. McKinney, F. Salmassi, and T. Warwick are with the Lawrence Berkeley National Laboratory, Berkeley, California 94720-8199. J. P. Metz and T. W. Tonnessen are with InSync, Inc., Albuquerque, New Mexico 87107.

Received 19 October 2005; revised 26 January 2006; accepted 30 January 2006; posted 6 February 2006 (Doc. ID 65462).

0003-6935/06/204833-10$15.00/0

© 2006 Optical Society of America

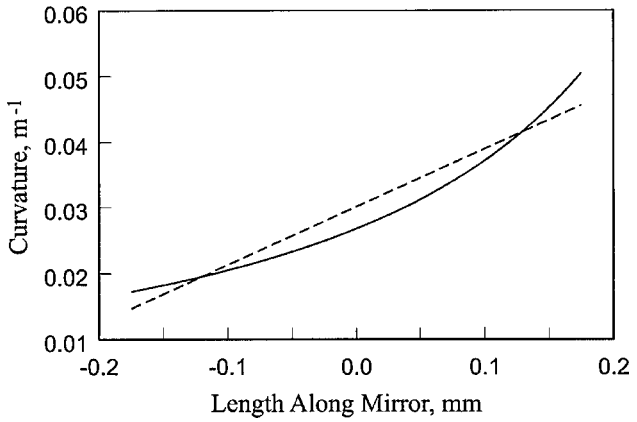

Fig. 1. Mirror shape required for perfect focusing, expressed as curvature versus length along the substrate. Dashed curve, best fit achievable with a uniform substrate.

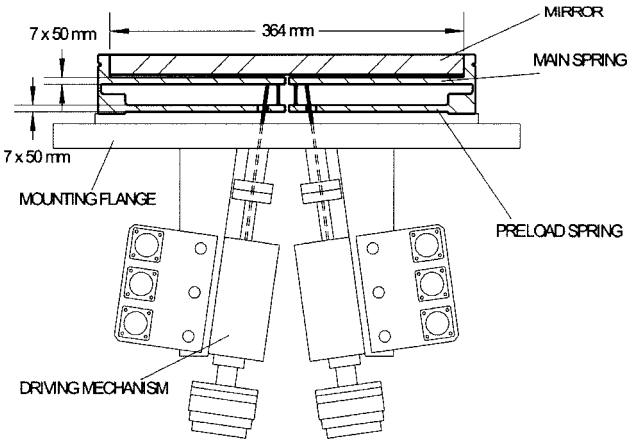

Fig. 2. Schematic of a flange-mounted bending mechanism, showing motorized drives, spring–pivot components in ultrahigh vacuum, and the mirror substrate to be bent. Further details can be found in Ref. 15.

coated polished SS (called throughout this paper Au-coated, polished SS) and from gold-coated polished electroless nickel plated onto SS (Au-coated Ni-plated SS), and report on the performance of the benders and the ultimate properties of the x-ray spot at the focus of the beam line.

2. Bender Mechanism and Substrate Stress

Here we discuss one of the three mirrors, focusing with a large demagnification factor of 43 and a working distance of 0.5 m. Figure 1 shows the required surface curvature. The dashed curve is the best fit with two tunable couples. We then achieve the desired elliptical shape by varying the width of the mirror along its length. Figure 2 shows the bender mechanism with the substrate in place. The substrate is 17-4PH SS, 350 mm long, 50 mm wide, and 20 mm thick. The 7 mm SS (17-4PH) main spring has a deflection of $Wl^3/(3EI)$, with $I = wt^3/12$. (W is the pulling force, up to 1000 N; w, t, and l are the width, thickness, and length, respectively, along the substrate; and E is the elastic modulus of the material.) The deflection at the end of the spring is ~7 mm. The maximum stress at the fixed end, $Wlt/(2l)$, is 4.5×10^8 N m^{-2} (or 60 ksi). This is just acceptable, as the practical limit against plastic deformation is ~90 ksi. The mirror stress is one fifth of this. The use of 17-4PH SS for the mirror substrate ensures that the polished shape (flat) converts properly into a tangential ellipse even when the substrate is stressed at this level. Mechanical details related to the bender mirror can be found in Ref. 15.

3. Measured Surface Roughness

The surface roughness measurements were performed with two instruments and techniques available at the Lawrence Berkeley National Laboratory (LBNL). An interferometric microscope [Micromap-570 (Ref. 29)] with five interchangeable objectives 2.5×, 5×, 10×, 20×, and 50×) at the ALS Optical Metrology Laboratory (OML) covers a range of spatial frequencies from 4×10^{-4} to 2 μm^{-1} (see Subsection 3.A below). An atomic-force microscope [AFM; Digital Instruments 3100 (Ref. 30)] at the Center for X-Ray Optics (CXRO) nanofabrication facility provides investigation of the mirror surface finish over an area of 5 μm × 5 μm to 100 μm × 100 μm, covering the spatial frequency range from approximately 0.1 to 50 μm^{-1} (see Subsection 3.B below). For a more sophisticated characterization of the mirror finishes, the surface height distributions measured with these microscopes were transformed into two-dimensional (2D) power spectral density (PSD) functions.[31] The roughness values were estimated based on the obtained 2D PSD distributions.

X-ray reflectivity and scattering measurements were performed at CXRO reflectometry and scattering beam line 6.3.2 at the ALS. Such measurements can also be converted into PSD spectra for the spatial frequency range from 0.1 to 100 μm^{-1} for 100–1000 eV x rays.[32,33] This frequency range almost coincides with the AFM range. At the lower frequencies, 0.1 to 2 μm^{-1}, the range overlaps the Micromap-570 interferometric microscope measurements. It is possible to cross check these PSD measurement techniques and eliminate the effects related to the modulation transfer function (MTF) of the instruments.

A 2D PSD function is a Fourier decomposition of the 2D surface height distribution into harmonic basis functions.[31] Its use is preferred to characterization of the surface finish by the parameters of rms roughness and correlation length.[34] X-ray scattering calculations based on a 2D PSD can be used to evaluate more reliably the in-plane and out-of-plane distributions of the x rays scattered by the optics because the PSD inherently contains more information than rms roughness or correlation lengths. These quantities are derived by integration from the PSD, which destroys information, and they are dependent on the choice of integration bandwidths. The corresponding scattering calculation when only these parameters are used is therefore less reliable, and only the evaluation of the integrated scattering can be performed.

A. Interferometric Microscope Measurements

The Micromap-570 interferometric microscope is a basic metrology tool for measuring microroughness of x-ray optics. The instrument at the LBNL OML has demonstrated measurements of subangstrom surface roughness. The measurement is in the form of a height distribution on a 2D surface grid that sets the maximum spatial frequency consistent with the magnification number of the objective used for measuring. A number of available objectives with magnification from 2.5× to 50× allow for measuring roughness over a spatial frequency range from 4×10^{-4} to 2 μm^{-1}. To suppress instrumental errors, we performed the measurements in supersmooth mode: In this mode an output height distribution $h_{m,n}$ is the result of two successive measurements over two different regions on the surface. The subscripts m and n count the pixels. The measured height distributions are subtracted one from another and renormalized to preserve the rms roughness (dispersion) of the resultant surface to be equal to the surface roughness of a single measurement:

$$h_{m,n} = (h_{1m,n} - h_{2m,n})/\sqrt{2}.$$

The standard output of the Micromap-570 microscope includes the values of roughness averaged over a specified area and averaged along a specified line. However, the 2D distribution of the surface height contains more information about the quality of the surface and can be used to derive a PSD distribution. The procedure and the software developed for converting the 2D surface height distribution measured with the Micromap-570 microscope into a 2D PSD distribution are described elsewhere.[35] Here we present the basic relations necessary for further consideration.

The 2D PSD function S_2 may be viewed as a Fourier decomposition of the 2D surface height distribution $h(x, y)$ into harmonic basis functions[36]:

$$S_2(u, v) = \lim_{A\to\infty}\left\langle \frac{1}{A}\left|\int_{-L_y/2}^{L_y/2} \mathrm{d}y \int_{-L_x/2}^{L_x/2} h(x, y) \times \exp[-i2\pi(sux + svy)]\mathrm{d}x\right|^2\right\rangle, \quad (1)$$

where L_x and L_y are the tangential and sagittal dimensions of the measured surface region, $A = L_xL_y$; u and v are the spatial frequency variables that correspond to the tangential x and sagittal y coordinates, respectively. In the case of discreet measurements with pixel dimensions Δx and Δy, M and N pixels in the tangential and sagittal directions, respectively, the 2D PSD distribution can be estimated from height distribution $h_{m,n}$ by the equation

$$S_2(l, k) = MN\Delta x\Delta y|F_{l,k}|^2, \quad (2)$$

where $F_{l,k}$ are the elements of the Fourier transform matrix

$$F_{l,k} = \frac{1}{M}\sum_{m=0}^{M-1}\left[\exp\left(\frac{-2\pi iml}{M}\right) \times \frac{1}{N}\sum_{n=0}^{N-1} h_{m,n}\exp\left(\frac{-2\pi ink}{N}\right)\right]. \quad (3)$$

The corresponding estimates of the tangential and sagittal one-dimensional (1D) two-sided PSDs, $S_1'(l)$ and $S_1'(k)$, are obtained by summing over rows (k) and columns (l), respectively. Here $0 \le l \le M - 1$ and $0 \le k \le N - 1$, and a prime signifies a two-sided PSD. These are then converted to one-sided PSDs (positive frequency only), just like those calculated from lines of surface heights directly:

$$S_1(l) = 2S_1'(l)g(l), \quad S_1(k) = 2S_1'(k)g(k), \quad (4)$$

where $0 \le l \le M/2$ and $0 \le k \le N/2$; $g(l) = 1/2$ at $l = 0, M/2$; $g(k) = 1/2$ at $k = 0, N/2$; and $g(l) = 1$ and $g(k) = 1$ otherwise. The reader is directed to Ref. 35, where details of the procedure are given.

To transform the area distribution of the residual surface heights available from the measurement with the Micromap-570 microscope into a 2D PSD distribution of the surface height, first we detrend a measured 2D height distribution with a best-fit 2D toroidal surface. The general expression for the toroidal surface is given by the expression

$$S(x, y) = k_{00} + k_{10}x + k_{20}x^2 + k_{01}y + k_{02}y^2 + k_{11}xy + k_{21}x^2y + k_{12}xy^2 + k_{22}x^2y^2. \quad (5)$$

Second, correction for the resolution asymmetry of the Micromap-570 interferometric microscope between the tangential and sagittal directions is performed. This asymmetry originates from the CCD camera readout through two independent channels with unbalanced amplification. To eliminate the related distortion of measured height distributions, the usual practice is to average the height distribution over two adjacent pixels in the sagittal direction. This averaging leads to a resolution asymmetry in the instrument, which is clearly seen by comparison of the tangential and sagittal 1D PSD spectra of a mirror with an isotropic finish. The asymmetry correction, based on a simple one-parameter analytical model,[35] allows us to account for the major effect of the averaging in the sagittal direction.

The dependence of the instrument's sensitivity on spatial frequency, which is usually characterized by a MTF,[37] leads to distortion of the measured PSD distribution compared with the PSD distribution that is intrinsic to the surface. Such a distortion is seen in a 1D PSD spectrum as a high-frequency roll-off (see Fig. 3). The PSD data presented throughout this section are not corrected for this effect. In Section 4 below, a comparison of PSD measurements made

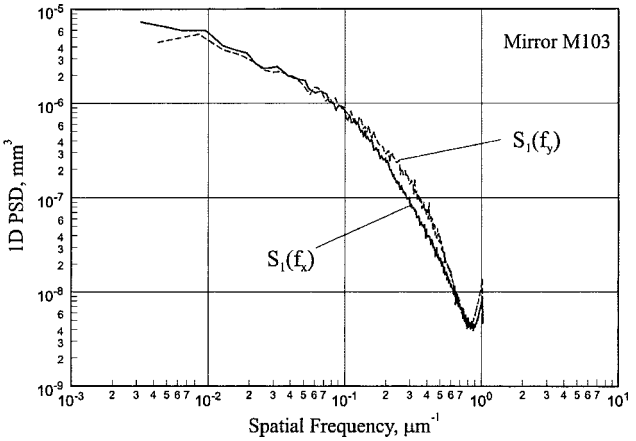

Fig. 3. 1D PSD spectra extracted from the 2D PSD distribution of the M103 Au-coated Ni-plated SS mirror measured with the Micromap-570 microscope with the 20× objective. Solid curve, tangential spectrum; dashed curve, sagittal spectrum. The spectra are the result of averaging over measurements of five different areas of the mirror surface. The roll-off seen at higher spatial frequencies is due to the MTF of the microscope. The hooklike features at the highest frequencies are artifacts of the correction of the CCD camera readout asymmetry (see text).

with the various techniques is shown to provide a method for finding the MTFs of the corresponding instruments. The effectiveness of the procedure developed for PSD presentation of the Micromap-570 measurements has also been demonstrated in Refs. 35 and 38 with a number of different x-ray optics, including mirrors and a grating.

We should mention that the correction implemented leads to hooklike artifacts in the corrected 1D PSD spectra that appear at the highest spatial frequencies (Fig. 3). For practical purposes these artifacts can be ignored because of their small magnitude (they are noticeable in Fig. 3 because of the log–log scale). It should be noted that a similar artifact was encountered in the early development of phase-shifted Fizeau

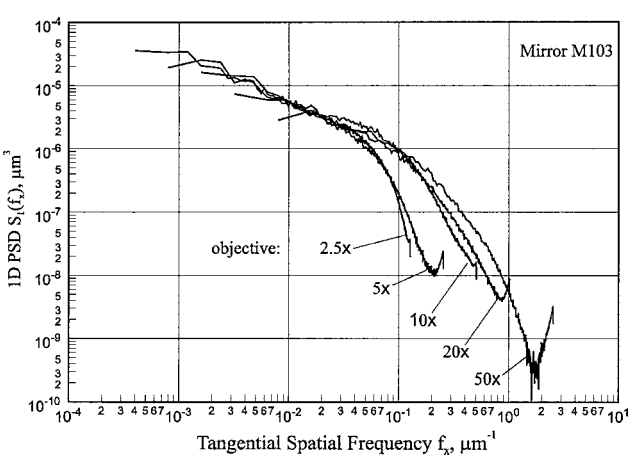

Fig. 4. 1D PSD spectra extracted from the 2D PSD distribution of the M103 Au-coated Ni-plated SS mirror measured with the Micromap-570 microscope with all available objectives. Each spectrum is the result of averaging over measurements of five different areas of the mirror surface.

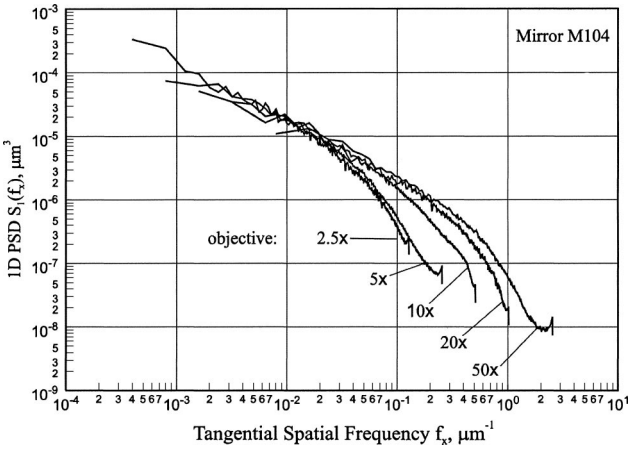

Fig. 5. 1D PSD spectra extracted from the 2D PSD distribution of the M104 Au-coated, polished SS mirror measured with the Micromap-570 microscope with all available objectives. Each spectrum is the result of averaging over measurements of five different areas of the mirror surface.

interferometers. Special methods for calibration of the MTF were proposed.[39] Unfortunately, no investigation of the origin of the artifact was reported.

Finally, we reproduce the expressions that give the surface rms roughness values from the tangential and sagittal 1D PSDs:

$$R_x = \left[\sum_{l=0}^{M/2} S_1(l)\Delta f_x\right]^{1/2}, \quad R_y = \left[\sum_{k=0}^{N/2} S_1(k)\Delta f_y\right]^{1/2}. \quad (6)$$

In Eqs. (6), Δf_x and Δf_y are the spatial frequency intervals that correspond to $\Delta f_x = 1/(M\Delta x)$ and $\Delta f_y = 1/(N\Delta y)$. Note that Eqs. (6) differ from an analogous formula in Ref. 31 by a factor of $\sqrt{2}$. The difference is due to the difference between definitions of the 1D PSD distributions as a two-sided 1D PSD used in Ref. 31 and as a one-sided 1D PSD given by Eq. (4).

Figure 3 shows an example of the 1D PSD spectra extracted from the 2D PSD distribution of the Au-coated Ni-plated SS mirror measured with the Micromap-570 microscope with the 20× objective. The spectra are averaged over measurements of five different regions of the mirror surface. The close similarity of the tangential and sagittal 1D PSD spectra presented in Fig. 3 is a characteristic property of the three SS mirrors: M103 with a nickel plating and M104 and M105 without (we adopt the mirror labeling used on the corresponding ALS beam line). The isotropic mirror surface finish is observed by use of all objectives on the Micromap-570 microscope as well as with the AFM (see Section 4 below). The tangential 1D PSD spectra of the Au-coated Ni-plated SS mirror, measured with different Micromap-570 objectives, are presented in Fig. 4. Each spectrum is the result of a conversion [Eqs. (4)] of the corresponding averaged 2D PSD distribution. The 2D PSD measurements with different objectives extend the available spatial frequency range. A noticeable feature of such an extension is that the higher spatial frequency roll-off observed with a lower-resolution objective is

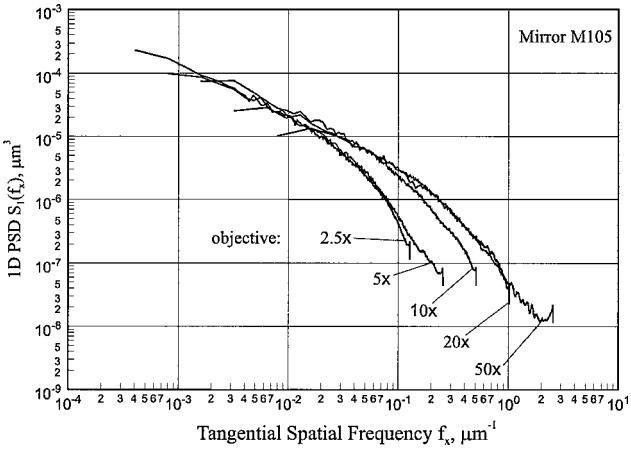

Fig. 6. 1D PSD spectra extracted from the 2D PSD distribution of the M105 Au-coated, polished SS mirror measured with the Micromap-570 microscope with all available objectives.

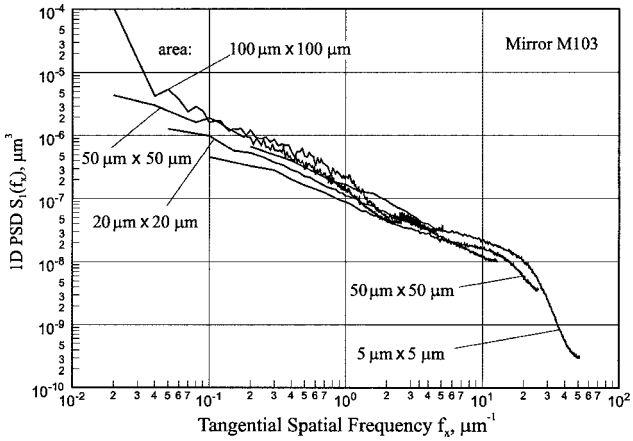

Fig. 7. 1D PSD spectra measured with the AFM instrument over different surface areas of the M103 Au-coated Ni-plated SS mirror. Each spectrum is a result of averaging over four measurements of different surface spots at the same AFM settings. The AFM measurements are rather consistent for measurements of areas of sizes from 5 μm × 5 μm to 100 μm × 100 μm. However, at lower spatial frequencies, 50 μm × 50 μm and 100 μm × 100 μm area measurements systematically yield larger 1D PSD values than the measurements over smaller areas.

corrected when one is measuring with a higher-resolution objective.

Compared to the Au-coated Ni-plated SS mirror (Fig. 4), the 1D PSD spectra measured or the mirrors with Au-coated, polished SS substrates (Figs. 5 and 6) have systematically larger magnitudes. The difference between the 1D PSD spectra of the two mirrors with Au-coated, polished SS substrates is significantly smaller.

Table 1 summarizes the result of the Micromap-570 measurements of the mirrors with the SS substrates in terms of rms surface roughness S_q, which is the standard deviation of the height values of the measured area from the best-fit second-order polynomial surface. The values of the roughness presented in the table are the Micromap-570 output parameters generated with the instrument's software.

B. Atomic-Force Microscope Measurements

The surface finishes of two of the mirrors were investigated with an AFM at the LBNL CXRO nanofabrication facility. These measurements were made of the Au-coated Ni-plated SS mirror and of one of the mirrors with a Au-coated, polished SS substrate. A series of AFM scans was performed with a Digital Instruments 3100 instrument with NanoScope software.[30] The AFM instrument operates with an atomically sharp tip oscillating at resonance above the surface to be measured. The amplitude of the oscillation is adjusted to bring the maximum excursion close to the surface, as the tip is raster scanned over the region of interest. By reflecting laser light off the back of the tip cantilever and into a detector system, the AFM instrument is able to resolve subnanometer changes in oscillation amplitude that correspond to changes in the height of the surface. Ordinary etched silicon cantilever tips with 15–20 nm tip diameters were used, with response frequencies of ~290 kHz. The AFM provides surface height distributions that can be converted, with the built-in software, into 1D PSD spectra and 2D PSD distributions. The instrument allows PSD measurements to be made for the approximate spatial frequency range from ~0.1 to ~50 μm^{-1}, which corresponds to a measuring surface area of as much as 100 μm × 100 μm with 512 × 512 elements. To produce an accurate characterization of the entire mirror surface, we carried out multiple measurements over different surface regions and calculated averaged PSD spectra (see Fig. 7). The 1D PSD spectra measured on the M104 mirror with a Au-coated, polished SS substrate are plotted in Fig. 8. These data were obtained in just a single measurement over each of the regions. As a result, the spread of data is increased. The lowest spatial frequency artifacts in

Table 1. Micromap-570 Measurements of the rms Surface Roughness of the Three Mirrors Described in This Paper

	rms Surface Roughness S_q (Å)				
Mirror	2.5× Objective	5× Objective	10× Objective	20× Objective	100× Objective
M103, Au-coated Ni-plated SS mirror[a]	5.3	5.1	7.3	5.4	5.7
M104, Au-coated, polished SS mirror	11.2	9.7	13.5	19.2	17.4
M105, Au-coated, polished SS mirror	9.6	10.8	13.1	17.2	13.7

[a]Here we keep the mirror labeling used on the corresponding ALS beam line.

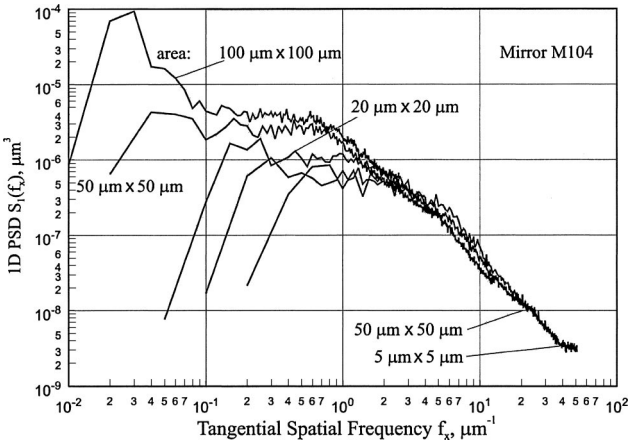

Fig. 8. 1D PSD spectra measured with the AFM instrument over different surface areas of the M104 Au-coated, polished SS mirror. The lowest spatial frequency artifacts are due to the detrending procedure with subtraction of a residual surface described with a third-power polynomial.

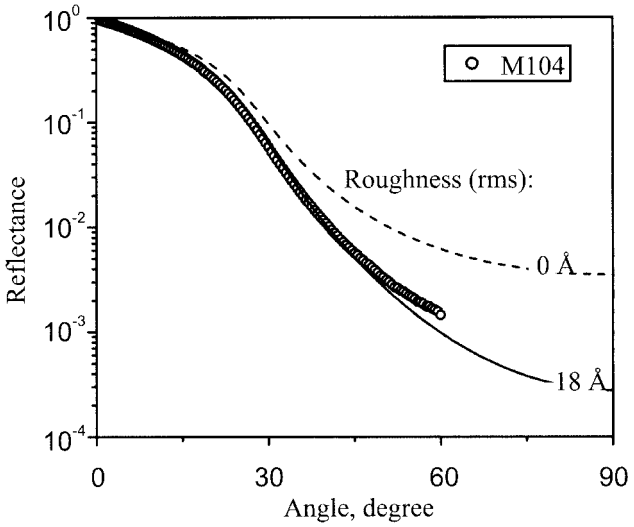

Fig. 9. X-ray reflectivity versus angle for the M104 Au-coated, polished SS mirror measured at 92 eV. Dashed curve, theoretical reflectivity of a perfectly smooth mirror; solid curve, fit to the measurements with a Nevot–Croce factor used to model the scattering loss and a rms roughness of 18 Å.

the 1D PSD spectra measured with this mirror are due to the detrending procedure with subtraction of a residual surface described by a third-order polynomial. Table 2 summarizes the result of the AFM measurements with the two mirrors in terms of rms surface roughness S_q. The values of the roughness presented in the table are the AFM output parameters generated with the instrument's software.

C. X-Ray Scattering and Reflectivity

The x-ray scattering and reflectivity measurements were performed with reflectometry and scattering beam line 6.3.2 (Refs. 40 and 41) at the ALS. The scattering measurements can be converted into the PSD spectra for the spatial frequency range from 0.1 to 100 μm^{-1} for 100–1000 eV x rays.

Figure 9 shows the reflectivity versus angle at 92 eV for the Au-coated, polished SS mirror M104. The reflectivity of an ideally smooth surface is shown by the dashed curve, and the solid curve is a fit to the data by use of a Nevot-Croce factor and a roughness of 1.8 nm. Figure 10 shows measured reflectivity for the M104 Au-coated polished SS mirror and the M103 Au-coated Ni-plated SS mirror. The reflectivity versus energy of the Au-coated, polished SS mirror follows very closely the theoretical reflectance curve of the Nevot-Croce model and has a rms roughness of 2 nm, consistent with the measurement of Fig. 9. The measured reflectivity of the Au-coated Ni-plated SS mirror is close to that of an ideal surface. Note that, with a high-quality surface finish such as that found on the Au-coated Ni-plated SS mirror, the reflectance measurement is rather insensitive to the surface roughness.[42]

The rms roughness deduced from the reflectivity measurements describes the reflectance loss that is due to x rays scattered out of the acceptance of the detector. It is therefore related to the high spatial frequency roughness. The exact frequency range depends on the incident angle, the angular acceptance of the detector, and the photon energy. For example, at 500 eV, integrating the PSD of the M104 mirror over the frequency range that scatters light out of the 1.2° half-angle detector acceptance gives a rms roughness of 21 Å (1 Å = 0.1 nm), consistent with the value obtained from the reflectivity measurements.

The angle-dependent scattering was measured for the M104 mirror with a Au-coated, polished SS substrate. Scattering measurements were performed at x-ray beam incidence angles of 1.5° and 5° and a photon energy of 92 eV. The PSD spectra deduced

Table 2. AFM Measurements of the Surface Roughness (rms) of Two of the Mirrors

	rms Surface Roughness S_q (Å)				
Mirror	5 μm × 5 μm Area	10 μm × 10 μm Area	20 μm × 20 μm Area	50 μm × 50 μm Area	100 μm × 100 μm Area
M103, Au-coated Ni-plated SS mirror	6.8	6.4	6.2	9.2	15.7
M104, Au-coated, polished SS mirror	16.4	15.3	14.9	14.2	18.0

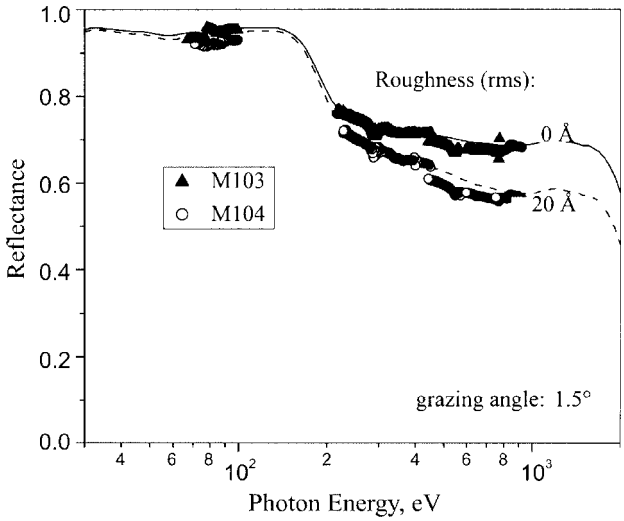

Fig. 10. Dependence on x-ray energy of the surface reflectance measured with the M103 Au-coated Ni-plated SS mirror and the M104 Au-coated, polished SS mirror. The solid and dashed curves represent the theoretical spectra computed from tabulated optical properties of gold, with a Nevot–Croce treatment of the loss that is due to surface roughness, assuming a mirror surface roughnesses of 5 Å for Au-coated Ni-plated SS mirror M103 and of 20 Å for Au-coated, polished SS mirror M104. The steel reflectivity is reduced above 200 eV by surface roughness effects.

from the scattering measurements of the M104 mirror are shown in Fig. 11.

4. Power-Law Approximation of Measured Power Spectral Density Distributions

Figures 12 and 13 present the 1D PSD spectra obtained from the Au-coated Ni-plated mirror M103 and from the Au-coated, polished SS mirror M104, respectively. Figure 12 presents the spectra obtained with the AFM and the Micromap interferometer. In Fig. 13 the measurements performed with the three different techniques, including the x-ray scattering

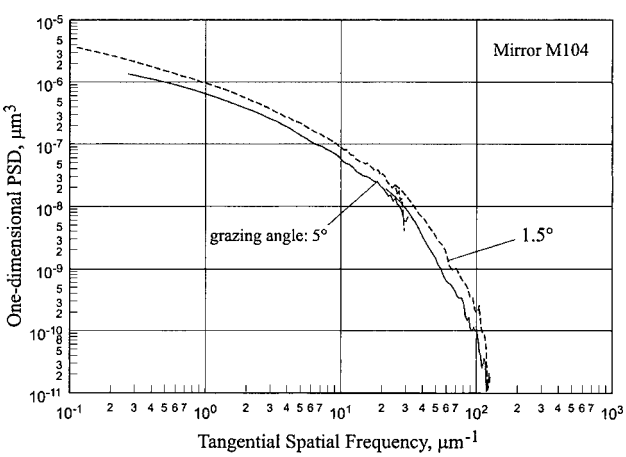

Fig. 11. 1D PSD spectra extracted from the x-ray scattering measurements with the M104 Au-coated, polished SS mirror. Solid curve, x-ray beam grazing-incidence angle of 1.5°; dashed curve, beam grazing angle of 5°. The measurements were performed at photon energy of 92 eV.

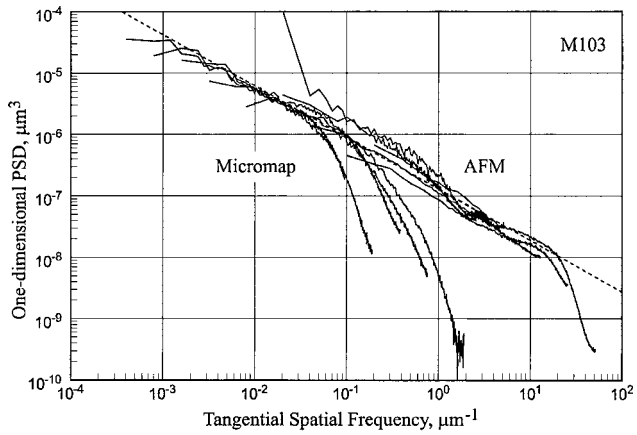

Fig. 12. Tangential 1D PSD spectra obtained with the M103 Ni-plated mirror. The spectra at lower spatial frequencies show measurements with different objectives of the interferometric microscope (cf. Fig. 4); the spectra at higher spatial frequencies represent the AFM data (cf. Fig. 7). Dashed curve, inverse power-law spectrum enveloping all the measured spectra. Note that the parameters of the inverse power-law spectrum (Table 3) are the same as for the sagittal 1D PSD spectra measured with the Micromap microscope and the AFM.

measurements, are shown. The AFM spatial frequency range almost coincides with the frequency range of the x-ray scattering experiment. It also overlaps at the lower frequencies with the Micromap-570 interferometric microscope measurements. This allows for cross checking the techniques.

We conclude from the cross check that all three techniques provide essentially consistent results. Moreover, for both mirrors the PSD spectra in the

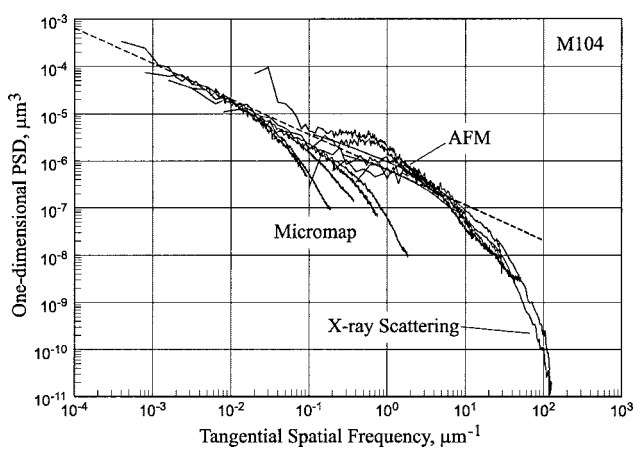

Fig. 13. Tangential 1D PSD spectra obtained with the Au-coated, polished SS M104. The spectra at lower spatial frequencies show measurements with different objectives of the interferometric microscope (cf. Fig. 5); the spectra at the middle spatial frequencies represent the AFM data (cf. Fig. 8); the spectra extracted from the x-ray scattering measurements cover the highest frequencies available. Dashed curve, inverse power-law spectrum enveloping all the measured spectra. Note that the parameters of the inverse power-law spectrum (Table 3) are the same as for the sagittal 1D PSD spectra measured with the Micromap microscope and the AFM.

Table 3. Measured Power-Law Parameters Obtained for the Frequency Range from Approximately 3×10^{-4} to 10 μm^{-1} and Corresponding Roughness Calculated over Frequency Range Characteristic for the 5× Objective

Mirror	Spectral Intensity S_1 (μm^3)	Spectral Index γ	rms Roughness S_q (Å)
M103, Au-coated Ni-plated SS mirror	1.3×10^{-7}	0.838	6.4
M104, Au-coated, polished SS mirror	6.5×10^{-7}	0.75	10.8
M105, Au-coated, polished SS mirror	5.5×10^{-7}	0.83	13.0

range of spatial frequencies from 3×10^{-4} to 10 μm^{-1} can be approximated with a power-law dependence, which is a straight line in the log–log scale used for Figs. 12 and 13. The power-law approximation has been found to be applicable to the PSD spectra of the high-quality x-ray mirrors made of polished glass ceramics (SiC) and metals.[43,44]

The power-law approximation has two parameters, spectral intensity $S_1(1)$ and spectral index γ:

$$S_1(f_x) = S_1(1)/f_x^{\gamma}, \tag{7}$$

where f_x is the tangential spatial frequency and subscript 1 is used to emphasize that $S_1(f_x)$ is a 1D PSD function; $S_1(1)$ is a constant equal to $S_1(f_x)$ at $f_x = 1\ \mu m^{-1}$. For the mirrors measured here, the power-law parameters were found from a linear envelope over the corresponding set of 1D PSD spectra (see, e.g., Figs. 12 and 13) plotted by eye. (A more sophisticated procedure based on fitting with weighting of the points of a measured 2D PSD distribution is under development.) The parameters are presented in Table 3. The values of the parameters are given assuming that all dimensional quantities are expressed in micrometers: $[S_1(f_x)] = \mu m^3$, $[f_x] = \mu m^{-1}$.

The spectral indices found for the mirrors under investigation here are too small to be consistent with the concept of a fractal surface finish.[34] A fractal profile (with spectral power of 1–3) has statistical properties that stay the same for scaling along the surface by a factor of ξ and for scaling of the height by a factor of $\xi^{(\gamma-1)/2}$. This can be thought of as an absence of internal length scales for the fractal profile determined by polishing.[34] In our case, the spatial frequency range investigated extends to frequencies high enough that the scale of the polishing process is important, leading to spectral indices smaller than 1.

For the inverse-power-law-like surfaces with parameters given in Table 3, the roughness values can be calculated from the corresponding discrete 1D PSD spectrum with Eq. (6). The results of such a calculation for the frequency interval and range corresponding to the Micromap measurements with the 5× objective are presented in Table 3. The roughness values shown in Table 3 have good agreement with the magnitudes presented in Tables 1 and 2. However, the results in Table 3 are considered significantly more reliable because of correction of the error that is due to the instrumental MTF.

5. Conclusions

We have shown that the surface finish of a stainless-steel mirror is significantly improved if, instead of a polished steel surface, an additional layer of nickel is applied and polished. The investigation is based on measured power spectral density spectra over a broad range of spatial frequencies from 3×10^{-4} to 10 μm^{-1}, available with three experimental instruments. These instruments are the Micromap-570 interferometric microscope, the Digital Instruments 3100 atomic-force microscope, and an experimental facility for measuring x-ray scattering and reflectivity. With all three mirrors investigated, the instruments provide essentially consistent results.

It was demonstrated that a power-law-like topography gives a good approximation for the measured PSD spectra over the broad range of spatial frequencies from $\sim 3 \times 10^{-4}$ to 10 μm^{-1}. The spectral index parameters that characterize the power-law-like envelopes of the experimental PSD spectra were found to be smaller than 1, which is the lower limit for the application of a fractallike description of the highly polished surface.[34] This can be thought of as a manifestation of a length scale related to polishing at high spatial frequencies.

We used the parameters found for the power-law approximation to obtain values of the surface roughness that were free of errors caused by the instrumental MTFs. The roughness of the polished nickel surface was evaluated to be ~6.4 Å, smaller by a factor of approximately 2 than the Au-coated, polished SS surface. This improvement decreases the scattering of x rays, as demonstrated with the x-ray reflectivity experiments described in Section 3.

We emphasize that the AFM and x-ray scattering measurements, which offer higher spatial resolution than measurements with the interferometric microscope, can be used to determine the Micromap-570 MTF and can be used to correct the high-frequency roll-off of the instrument.[38]

We are grateful to Eugene Church, Howard Padmore, and Peter Takacs for useful discussions and to Nord Andersen and Troy Stevens for mirror bender design. The ALS is supported by the Director, Office of Science, Office of Basic Energy Sciences, Materials Science Division, U.S. Department of Energy, under contract DE-AC02-05CH11231 with the Lawrence Berkeley National Laboratory.

References

1. A. Bianco, G. Sostero, and D. Cocco, "Kirkpatrick–Baez elliptical bendable mirrors at the nanospectroscopy beamline: metrological results and x-rays performance," in *X-Ray Mirrors, Crystals, and Multilayers II,* A. K. Freund, A. T. Macrander, T. Ishikawa, and J. L. Wood, eds., Proc. SPIE **4782,** 74–85 (2002).
2. S. J. Chen, C. K. Kuan, S. Y. Perng, D. J. Wang, H. C. Ho,

T. C. Tseng, Y. C. Lo, and C. T. Chen, "New focusing mirror system for synchrotron radiation infrared beamlines," Opt. Eng. **43,** 3077–3082 (2004).
3. Y. Dabin, G. Rostaing, O. Hignette, A. Rommeveaux, and A. K. Freund, "The present state of Kirkpatrick–Baez mirror systems at the ESRF," in *X-Ray Mirrors, Crystals, and Multilayers I,* A. K. Freund, A. T. Macrander, T. Ishikawa, and J. L. Wood, eds., Proc. SPIE **4782,** 235–245 (2002).
4. A. K. Freund, "Recent progress in x-ray optics at the ESRF," J. Phys. IV **104,** 165–170 (2003).
5. A. Freund, "Challenges for synchrotron x-ray optics," in *X-Ray Mirrors, Crystals, and Multilayers I,* A. K. Freund, A. T. Macrander, T. Ishikawa, and J. L. Wood, eds., Proc. SPIE **4782,** 1–11 (2002).
6. P. A. Heimann, H. A. Padmore, and A. A. Zholents, "X-ray optical designs for the Linac-based Ultrafast X-ray source (LUX)," in *Fourth-Generation X-Ray Sources and Ultrafast X-Ray Detectors*, R. O. Tatchyn, Z. Chang, J.-C. Kieffer, and J. B. Hastings, eds., Proc. SPIE **5194,** 39–45 (2004).
7. O. Hignette, P. Cloetens, W.-K. Lee, W. Ludwig, and G. Rostaing, "Hard x-ray microscopy with reflecting mirrors status and perspectives of the ESRF technology," J. Phys. IV **104,** 231–234 (2003).
8. G. E. Ice, E. D. Specht, J. Z. Tischler, A. M. Khounsary, L. Assoufid, and C. Liu, "At the limit of nondispersive micro- and nanofocusing mirror optics," in *Micromachining Technology for Micro-Optics and Nano-Optics II,* E. G. Johnson and G. P. Nordin, eds., Proc. SPIE **5347,** 1–8 (2004).
9. M. Janousch, A.-M. Flank, P. Lagarde, G. Cauchon, S. Bac, J. M. Dubuisson, Th. Schmidt, R. Wetter, G. Grolimund, and A. M. Scheidegger, "LUCIA—a new 1–7 keV μ-XAS beamline," in *Synchrotron Radiation Instrumentation,* T. Warwick, J. Arthur, H. A. Padmore, and J. Stöhr, eds., AIP Proc. **705,** 312–315 (2004).
10. A. M. Khounsary, G. E. Ice, and P. J. Eng, "Mirrors for nanofocusing x-ray beams," in *X-Ray Mirrors, Crystals, and Multilayers II,* A. K. Freund, A. T. Macrander, T. Ishikawa, and J. L. Wood, eds., Proc. SPIE **4782,** 65–73 (2002).
11. P. P. Naulleau, P. Batson, P. Denham, D. Richardson, and J. Underwood, "An *in situ* scanning-slit alignment system for Kirkpatrick–Baez optics," Opt. Commun. **212,** 225–233 (2002).
12. N. A. Papadogiannis, L. A. A. Nikolopoulos, D. Charalambidis, G. D. Tsakiris, P. Tzallas, and K. Witte, "On the feasibility of performing nonlinear autocorrelation with attosecond pulse trains," Appl. Phys. B **76,** 721–727 (2003).
13. I. K. Robinson, F. Pfeiffer, I. A. Vartanyants, S. Yugang, and X. Younan, "Enhancement of coherent x-ray diffraction from nanocrystals by introduction of x-ray optics," Opt. Express **11,** 2329–2334 (2003).
14. R. Spolenak, N. Tamura, B. C. Valek, A. A. MacDowel, R. S. Celestre, H. A. Padmore, W. L. Brown, T. Marieb, B. W. Batterman, and J. R. Patel, "High resolution microdiffraction studies using synchrotron radiation," in *Stress-Induced Phenomena in Metallization. Sixth International Workshop on Stress-Induced Phenomena in Metallization,* S. P. Baker, M. A. Korhonen, E. Arzt, and P. S. Ho, eds., AIP Proc. **612,** 217–228 (2002).
15. T. Warwick, N. Andresen, J. Comins, A. Franck, M. Gilles, T. Tonnessen, and T. Tyliszczak, "Large aperture micro-focus KB mirrors for spectroscopy experiments at the Advanced Light Source," in *Synchrotron Radiation Instrumentation,* T. Warwick, J. Arthur, H. A. Padmore, and J. Stöhr, eds., AIP Proc. **705,** 772–775 (2004).
16. X. Yu, Zh. Hu, H. Pan, Q. Wang, and P. Xu, "The re-design of a soft x-ray beamline for photoemission spectroscopy at NSRL," in *Synchrotron Radiation Instrumentation,* T. Warwick, J. Arthur, H. A. Padmore, and J. Stöhr, eds., AIP Proc. **705,** 396–399 (2004).
17. K. Yamamura, H. Mimura, K. Yamauchi, Y. Sano, A. Saito, T. Kinoshita, K. Endo, Y. Mori, A. Souvorov, M. Yabashi, K. Tamasaku, and T. Ishikawa, "Aspheric surface fabrication in nm-level accuracy by numerically controlled plasma chemical vaporization machining (CVM) and elastic emission machining (EEM)," in *X-Ray Mirrors, Crystals, and Multilayers I,* A. K. Freund, A. T. Macrander, T. Ishikawa, and J. L. Wood, eds., Proc. SPIE **4782,** 265–270 (2002).
18. K. Yamamura, K. Yamauchi, H. Mimura, Y. Sano, A. Saito, K. Endo, A. Souvorov, M. Yabashi, K. Tamasaku, T. Ishikawa, and Y. Mori, "Fabrication of elliptical mirror at nanometer-level accuracy for hard x-ray focusing by numerically controlled plasma chemical vaporization machining," Rev. Sci. Instrum. **74,** 4549–4553 (2003).
19. E. Ziegler, T. Bigault, and J. Hoszowska, "An x-ray focusing system combining a sagittally bent crystal and a Kirkpatrick–Baez system," in *Synchrotron Radiation Instrumentation,* T. Warwick, J. Arthur, H. A. Padmore, and J. Stöhr, eds., AIP Proc. **705,** 768–771 (2004).
20. E. Ziegler, J. Hoszowska, T. Bigault, L. Peverini, J. Y. Massonnat, and R. Hustache, "The ESRF BM05 metrology beamline: instrumentation and performance upgrade," in *Synchrotron Radiation Instrumentation,* T. Warwick, J. Arthur, H. A. Padmore, and J. Stöhr, eds., AIP Proc. **705,** 436–439 (2004).
21. L. H. Underwood, "Generation of a parallel x-ray beam and its use for testing collimators," Space Sci. Instrum. **3,** 259–270 (1977).
22. L. H. Underwood and D. Turner, "Bend glass optics," in *X-Ray Imaging,* R. C. Chase and G. W. Kuswa, eds., Proc. SPIE **106,** 125–135 (1977).
23. J. J. Ferme, "New improvements in bendable mirrors," in *Materials, Manufacturing, and Measurement for Synchrotron Radiation Mirrors,* P. Z. Takacs and T. W. Tonnessen, eds., Proc. SPIE **3152,** 103–111 (1997).
24. N. D. Hartman, P. A. Heimann, A. A. MacDowell, K. D. Franck, A. P. Grieshop, S. C. Irick, and H. A. Padmore, "Design, analysis, and performance of an epoxy-bonded bendable mirror," in *Advances in Mirror Technology for Synchrotron X-Ray and Laser Applications,* A. M. Khounsary, eds., Proc. SPIE **3447,** 40–51 (1998).
25. M. R. Howells, "Design strategies for monolithic adjustable-radius metal mirrors," Opt. Eng. **34,** 410–417 (1995).
26. E. Morikawa, J. D. Scott, and V. Saile, "Adaptive optics for resolution/throughput optimization; variable-radius-mirror application for a PGM," Nucl. Instrum. Methods A **319,** 116–120 (1992).
27. R. Seungyn, S. Locklin, S. Irick, and M. Howells, "New schemes in the adjustment of bendable elliptical mirrors using a long trace profiler," in *Materials, Manufacturing, and Measurement for Synchrotron Radiation Mirrors,* P. Z. Takacs and T. W. Tonnessen, eds., Proc. SPIE **3152,** 112–119 (1997).
28. O. Hignette, G. Rostaing, P. Cloetens, A. Rommeveaux, W. Ludwig, and A. Freund, "Submicron focusing of hard x-rays with reflecting surfaces at the ESRF," in *X-Ray Micro- and Nano-Focusing: Applications and Techniques II,* I. McNulty, ed., Proc. SPIE **4499,** 105–116 (2001).
29. Micromap Corporation, Tucson, Ariz.
30. Digital Instruments/Veeco Instruments, Inc., Woodbury, New York.
31. J. C. Stover, *Optical Scattering: Measurement and Analysis* (SPIE Optical Engineering Press, 1995).
32. J. V. Bixler, C. W. Mauche, C. J. Hailey, and L. Medison, "Reflectivity and scattering measurements of an advanced x-ray astrophysics facility test coating sample," Appl. Opt. **34,** 6542–6551 (1995).
33. V. E. Asadchikov, I. V. Kozhevnikov, Yu. S. Krivonosov, R. Mercier, T. H. Metzger, C. Morawe, and E. Ziegler, "Applica-

tion of x-ray scattering technique to the study of supersmooth surfaces," Nucl. Instrum. Methods A **530,** 575–595 (2004).
34. E. L. Church, "Fractal surface finish," Appl. Opt. **27,** 1518–1526 (1988).
35. V. V. Yashchuk, A. D. Franck, S. C. Irick, M. R. Howells, A. A. MacDowell, and W. R. McKinney, "Two dimensional power spectral density measurements of x-ray optics with the Micromap interferometric microscope," in *Nano- and Micro-Metrology*, H. Ottevaere, P. DeWolf, and D. S. Wiersma, eds., Proc. SPIE **5858,** 85–96 (2005).
36. R. N. Bracewell, *The Fourier Transform and Its Applications* (McGraw-Hill, 1986), pp. 108–112.
37. G. D. Boreman, *Modulation Transfer Function in Optical and Electro-Optical Systems* (SPIE Press, 2001).
38. V. V. Yashchuk, S. C. Irick, E. M. Gullikson, M. R. Howells, A. A. MacDowell, W. R. McKinney, F. Salmassi, and T. Warwick, "Cross-check of different techniques for two dimensional power spectral density measurements of x-ray optics," in *Advances in Metrology for X-Ray and EUV Optics,* L. Assoufid, P. Z. Takacs, and J. S. Taylor, eds., Proc. SPIE **5921,** 105–116 (2005).
39. G. Zhishan and C. Jinbang, "Calibration of frequency response function for a phase-shifted interferometer," in *Advanced Optical Manufacturing and Testing Technology 2000,* L. Yang, H. M. Pollicove, Q. Xin, and J. C. Wyant, eds., Proc. SPIE **4231,** 397–401 (2000).
40. Beam line 6.3.2 at the Center for X-Ray Optics, Materials Science Division, Lawrence Berkeley Laboratory, Berkeley, Calif., http://www.cxro.lbl.gov/als6.3.2.
41. J. H. Underwood and E. H. Gullikson, "High-resolution, high-flux, user friendly VLS beamline at the ALS for the 50–1300 eV energy region," J. Electron Spectrosc. Related Phenom. **92,** 265–272 (1988).
42. E. Gullikson, Center for X-Ray Optics, Lawrence Berkeley National Laboratory, Berkeley, California 94720 (personal communication, 2005), http://www.cxro.lbl.gov/optical_constants/mirror2.html.
43. E. L. Church and P. Z. Takacs, "Surface scattering," in *Handbook of Optics,* 2nd ed., M. Bass, J. M. Enoch, E. W. Van Stryland, and W. L. Wolfe, eds. (McGraw-Hill, 2000), Vol. 1, Chap. 7.
44. P. Z. Takacs and E. L. Church, "Figure and finish of grazing-incidence mirrors," Nucl. Instrum. Methods A **291,** 253–264 (1990).